

Compact, Broadband and Reliable Lateral MEMS Switching Networks for 5G Communications

Sukomal Dey^{1, *}, Shiban K. Koul², Ajay K. Poddar³, and Ulrich Rohde³

Abstract—The design, development, and characterization of broadband (1–30 GHz) micro electromechanical systems (MEMS) based electrostatically driven lateral switching networks are presented in this paper. Initially, single switch performances are optimized, and later it is used to develop different switching networks like single-pole-double-throw (SPDT), single-pole-three-throw (SP3T), and single-pole-six-throw (SP6T). All switches are extensively characterized including reliability testing. Switching networks demonstrate measured return loss of better than 21 dB (11.4 dB) with worst case insertion loss of 0.67 dB (~ 5 dB) and isolation of better than 31 dB (17.7 dB) at 3.5 GHz (28 GHz) for 5G communications. Switching networks tested for > 1 billion cycles with 1 W of RF power are found to be operational. Maximum fabricated switch (SP6T) area is ~ 0.7 mm² including bias lines and pads.

1. INTRODUCTION

In fifth-generation (5G) communication, the radio frequency (RF) main path simultaneously transmits and receives RF signals. Figure 1(a) shows the direct conversion radio architecture used widely at sub-6 GHz for radio frequency front end (RFFE). Low-noise amplifier Multiplex Module (LMM) RFFE used in millimeter wave 5G is efficient for downlink and uplink carrier aggregations, as shown in Figure 1(b). In both the cases depicted in Figure 1, single-pole-multi-throw (SP n T) switching networks play a crucial role. Different technologies have been used globally for the development of SP n T switches using (a) PiN diodes, (b) CMOS, and (c) micromachining technologies. Among all, RF micromachine based SP n T switches have attracted attention due to their low power consumption, low loss, good linearity, and excellent isolation while operating with multiple ports at a time over a wide band [1].

Lateral switches have attracted considerable attentions as the strongest alternatives to the conventional vertically driven MEMS switches owing to their high broadband isolation and no dielectric charging properties. The performance of the contact type lateral MEMS switches are investigated by different research groups, and most variants are implemented in coplanar waveguide (CPW) transmission line. These switches demonstrate in-plane design flexibility, reliable mechanical stability, and high reliability [1–5].

The work reported here greatly improves the overall performance of four variants of the SP n T community (where $n = 2, 3,$ and 6). The work is divided into three phases. Phase I provides brief descriptions on the fabrication process, and the same process is used to develop all switching networks. Phase II describes single lateral switch performances which is the functional building block in SP n T networks. Phase III focuses on design and measurements on SP n T MEMS switches. Finally, phase IV describes reliability performances of switches followed by the state-of-the-art comparisons.

Received 17 September 2019, Accepted 19 November 2019, Scheduled 25 November 2019

* Corresponding author: Sukomal Dey (sukomal28@gmail.com).

¹ Department of Electrical Engineering, Indian Institute of Technology Palakkad, India. ² Centre for Applied Research in Electronics, Indian Institute of Technology Delhi, India. ³ Synergy Microwave Corporation, NJ, USA.

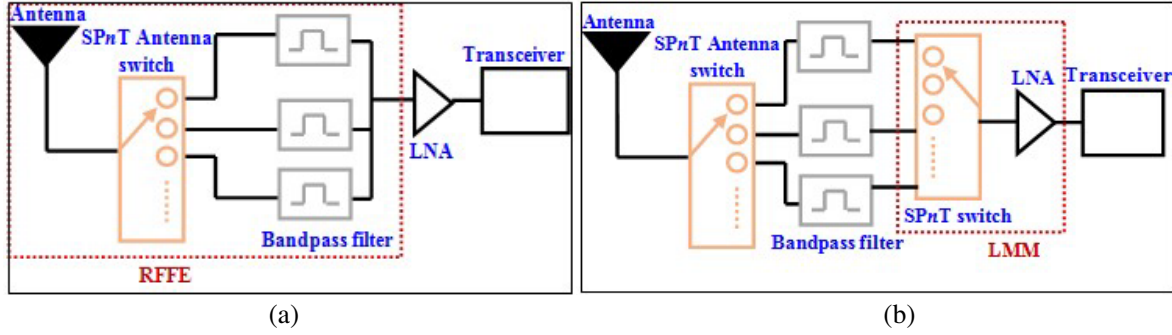


Figure 1. Simplified (a) Direct conversion receiver block diagram used at sub-6 GHz and (b) low-noise amplifier Multiplex Module (LMM) for millimeter wave.

2. FABRICATION PROCESS: PHASE-I

The device is fabricated on a $635\ \mu\text{m}$ alumina substrate ($\epsilon_r = 9.8$) after RCA cleaning of the wafer. The full fabrication process was reported in detail in [6]. In brief, initially $70\ \text{nm}$ Titanium Tungsten (TiW) is sputtered (using lift-off) [Figure 2(a)], and a $0.5\ \mu\text{m}$ SiO_2 layer is deposited and patterned on the TiW [Figure 2(b)]. Later, $2\ \mu\text{m}$ gold is electroplated to form fixed electrode and CPW lines [Figure 2(c)]. A $2.5\ \mu\text{m}$ spin coated Polyimide (PI) is coated, and anchor holes openings are made on the PI layer [Figure 2(d)]. A gold seed layer for electroplating is sputtered on the PI layer, and $3.5\text{--}4\ \mu\text{m}$ beam is electroplated [Figure 2(e)]. Finally, the sacrificial layer is released using CO_2 Critical Point Drying (CPD) process at 350°C in the oven and etched using EKC 265 [Figure 2(f)]. The fabrication process steps are shown in Figure 2. The yield is limited by the CPD process as well as the type of geometries in the layout. Generally, yield is more than 80% in this phase of the fabrication.

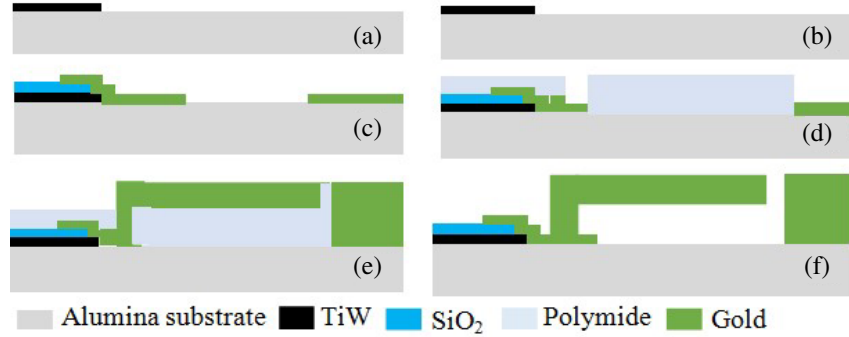


Figure 2. Schematic of fabrication process steps.

3. DESIGN AND MEASUREMENTS OF SINGLE MEMS SWITCH: PHASE II

Microscopic images of the single lateral MEMS single switch is depicted in Figure 3(a). The lateral switch includes a $50\ \Omega$ coplanar waveguide (CPW) line ($G = 35\ \mu\text{m}$, $W = 80\ \mu\text{m}$) and a movable beam between the input and output ports on alumina substrate ($\epsilon_r = 9.8$). This movable beam is fixed at one port (input) and comes into contact with the output line based on electrostatic actuation. A spring is attached at the centre of the cantilever beam and is positioned between the cantilever beam and the ground of the CPW. The spring has a semitriangular shape and is optimized with different angle θ variations in electromechanical solvers. Finally, $\theta = 30^\circ$ gives optimum response in terms mechanical stability with dedicated bias post and robust movable beam as shown in Figure 3(a). All optimized switch dimensions are marked in Figure 3(a). The mechanical force of the spring provides an additional

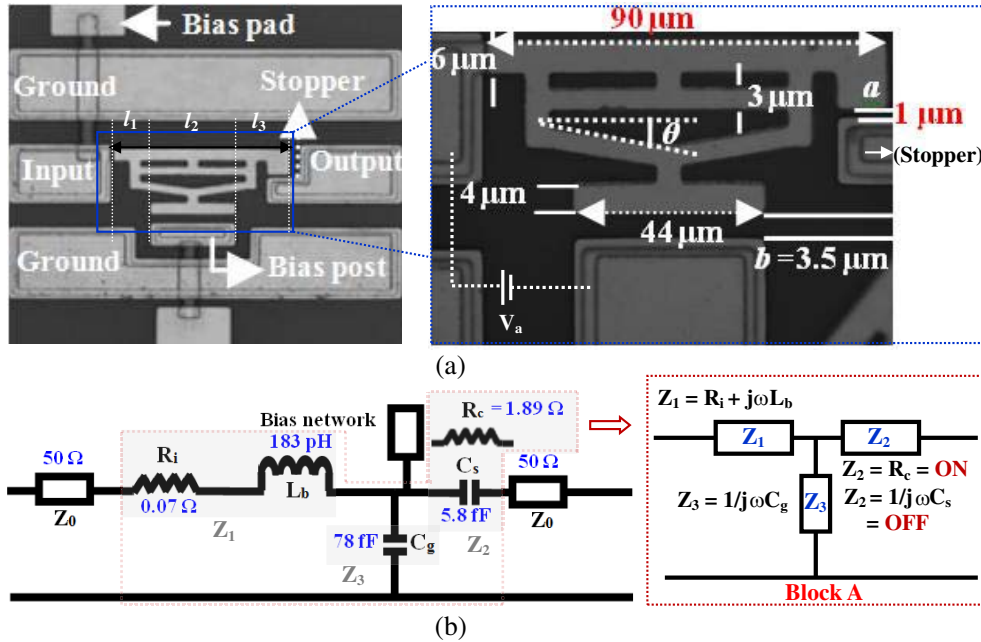


Figure 3. (a) SEM image of the fabricated lateral MEMS switch where all optimized structural parameters are marked and (b) its equivalent circuit model.

force to move the beam back to its rest position when the switch is in the OFF-state. The electrostatic actuation (V_a) between the center line of the beam and ground causes it to move in a lateral direction towards the mechanical stopper of the output port [see Figure 3(a)]. Note that when the beam moves, it is necessary to contact the second part of the center line without touching the ground line to avoid short circuited condition. Primary design criterion here is to keep $a \ll b$ where a (1 μm) is a distance between beam and mechanical stopper of the second port, and b (3.5–4 μm) is the distance between the mechanical spring and ground line, as shown in Figure 3(d). It substantially helps the switch to move within pull-in range and hence improves the reliability. Movable beam thickness is ~ 3.5 μm, and material is gold. The electromechanical modeling and dynamic analysis of the switch are given in [1].

If the total length (L) of the cantilever beam is divided in l_1 , l_2 , and l_3 , respectively, as shown in Figure 3(a), then total electrostatic force can be defined as

$$F_e = \int_{l_1}^{l_1+l_2} \frac{\epsilon_0 t V_a dx}{2(b-a)^2} \quad (1)$$

where ϵ_0 is the absolute permittivity, t the thickness, and V_a the actuation bias voltage.

The proposed lateral switch is inline in nature and has an extra spring that provides additional inductance. Hence, CPW ground lines beside the middle part of the cantilever beam are cut to avoid drastic increase in the characteristic impedance. Figure 3(b) shows the equivalent circuit of the lateral series switch. This model consists of two input and output CPW transmission lines with characteristic impedance (Z_0) of 50 Ω, cantilever beam of resistance (R_i), a cantilever beam line inductor (L), switch series capacitor, (C_s) at off-state or a ON-state switch contact resistor (R_c), and a shunt coupling capacitor (C_g). All circuit parameters are extracted from measured S -parameters using equations given in [1]. This circuit model forms a T-type model with Z_1 , Z_2 , and Z_3 impedances and depicted in Figure 3(b). Note that switch inductance (L_b) and CPW cut are optimized in an electromagnetic solver for optimum matching performance. As a result, simulated matching is better than 14 dB up to 30 GHz, as shown in Figure 4(d). Total area of the fabricated switch is $0.33 \times 0.19 \text{ mm}^2$.

After fabrication of the single switch, all performances are critically characterized. Negligible deflection (~ 40 nm) is observed at free end of the cantilever. Switch takes ~ 90 V to make proper contact with the output line with measured switching time of 38 μsec, and it takes ~ 57 μsec to settle in rest position, as depicted in Figures 4(a)–4(b), respectively. Figure 4(c) shows that measured mechanical

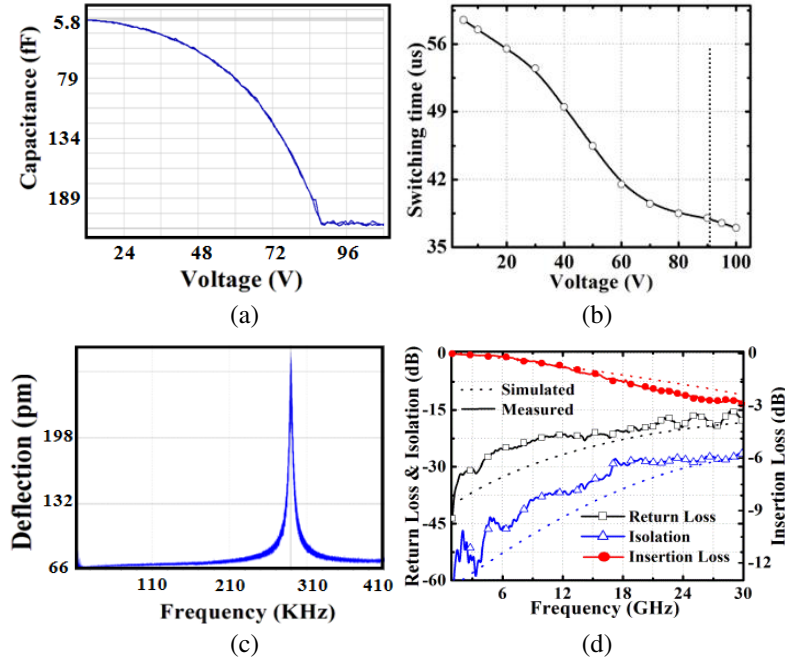


Figure 4. Measured (a) actuation voltage, (b) switching time, (c) mechanical resonance frequency and (d) *S*-parameter responses of the single lateral MEMS switch.

resonance frequency of the fabricated switch is 0.28 MHz. Finally, *S*-parameter performances of the single switch are tested up to 30 GHz using Agilent Vector Network Analyzer (E8361C) with cascade dc probes and calibrated using short-open-load-thru (SOLT) standard to the probe tips. Results are carefully observed at 3.5 GHz and 28 GHz, respectively for 5G applications. Switch demonstrates measured return loss of better than 30 dB (16.3 dB) with worst case insertion loss of 0.28 dB (2.82 dB) at 3.5 GHz (28 GHz), and isolation is better than 28 dB up to 30 GHz, as shown in Figure 4(d). Note that third-order inter-modulation intercept point (IIP3) is also tested on the switch using a two tone test with $f_1 = 1940$ MHz and $f_2 = 1980$ MHz, respectively. IIP3 measurement setup is reported in [4]. Switch shows IIP3 of ~ 37 dBm in the ON-state.

4. DESIGN AND TESTING OF MEMS SWITCHING NETWORKS: PHASE III

After successful fabrication and extensive characterization of single switch, different SP n T switching networks are fabricated. A simplified model of the SP n T switch is depicted in Figure 5. Microscopic image of the fabricated SPDT switch is shown in Figure 6(a) followed by *S*-parameter results. The total area of the fabricated SPDT switch is 0.25 mm². Switch includes a similar cantilever beam but with two

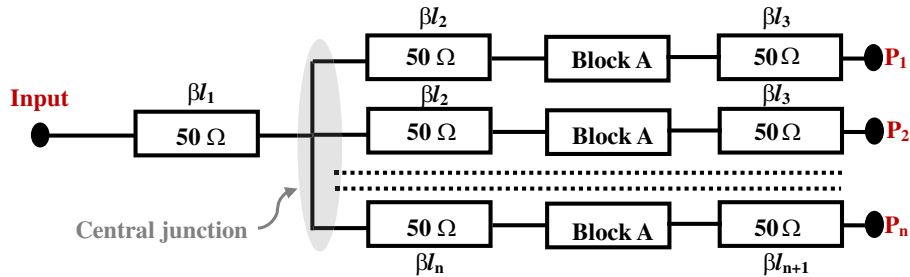


Figure 5. Simplified model of SP n T switch where Block A is defined in Figure 3(b).

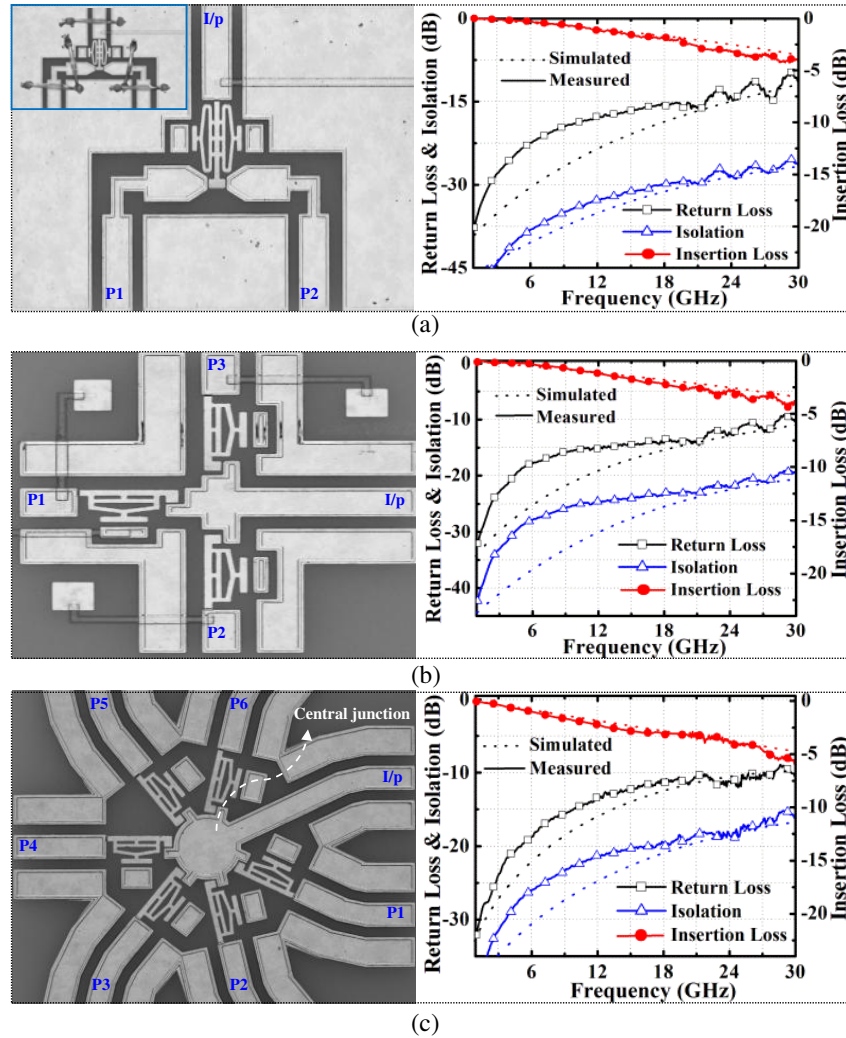


Figure 6. Microscopic images and measured versus simulated S -parameter responses of (a) SPDT, (b) SP3T and (c) SP6T MEMS switching networks.

similar kinds of springs laterally attached to either side of the beam. Two dedicated bias posts are used for actuation. The free end of the beam is able to deflect in either lateral direction based on dc bias and come in contact with a contact bump of either port, depending on the direction in which the cantilever beam deflects. At a given time, one of the actuators may be ON, while the other is OFF. Same design criteria are followed ($a \ll b$) in the SPDT switch followed by same structural dimensions. All CPW ground planes are connected with wire bonding to equalize the ground potential, as shown in the inset of Figure 6(a). SPDT switch gives measured return loss of better than 27 dB (11.6 dB) with worst case loss of 0.42 dB (3.3 dB) at 3.5 GHz (28 GHz) from all ports, and switch shows average isolation of better than 28 dB up to 30 GHz, as shown in Figure 6(b). Note that isolation is considerably higher in SPDT due to effective gap in one port doubling ($2 \mu\text{m}$) when other port is connected.

Microscopic images of SP3T and SP6T switches are shown in Figure 6(b) and Figure 6(c), respectively. The total area of the fabricated SP3T and SP6T switches are 0.36 mm^2 and 0.7 mm^2 , respectively. The input port of the SP3T (SP6T) lateral switch includes a central junction from which three (six) separate cantilever beams extend. All central junctions are optimized in full wave simulator (in terms of matching), and a similar actuation mechanism is followed. Each actuator is biased by a separate bias pad. Note that, at a given time, one of the actuators may be biased, such that the beam associated with that actuator is deflected and contacts corresponding output port. Nevertheless,

as SPDT, all CPW ground planes are connected with wire bonds in both switches (SP3T and SP6T). Finally, SP3T switch demonstrates measured average return loss of better than 22 dB (13 dB) with worst case average loss of 0.37 dB (3.89 dB) at 3.5 GHz (28 GHz) from all ports, as shown in Figure 6(b). Measured isolation is better than 33 dB (20 dB) at 3.5 GHz (28 GHz), as depicted in Figure 6(b). The SP6T switch performs well with return loss of better than 21 dB (11.4 dB), worst case insertion loss of 0.67 dB (~ 5 dB), and isolation of better than 31 dB (15 dB) from all six ports at 3.5 GHz (28 GHz), as shown in Figure 6(c).

Note that all measured responses presented in Figure 6 are validated using fitted parametric extraction model shown in Figure 5 with measured S -parameters data using Equations (2)–(3) for ON state condition, as stated below

$$S_{11} \approx \frac{R_t}{(2Z_0 + R_t)} \quad (2)$$

$$S_{21} \approx \frac{2Z_0}{(2Z_0 + R_t)} \quad (3)$$

where $R_t = R_i + R_c$. The OFF-state isolation (S_{21}) can be found considering Figure 3 as T-equivalent model, and S_{21} can be formulated using equations (4)–(5) as given below

$$S_{21} = \frac{2Z_0Z_3}{2Z_0Z_3 + Z_0(Z_0 + Z_1 + Z_2) + (Z_1Z_2 + Z_2Z_3 + Z_3Z_1)} \quad (4)$$

where

$$\begin{aligned} Z_1 &= R_i + j\omega L_b \\ \text{OFF-state: } Z_2 &= \frac{1}{j\omega C_s} \\ \text{ON-state: } Z_2 &= R_c \\ Z_3 &= \frac{1}{j\omega C_g} \end{aligned}$$

Note that switch capacitance (C_s) plays a role in OFF state, and isolation can be approximated as,

$$S_{21} \approx j2\omega C_s Z_0 \quad (5)$$

when

$$S_{21} \ll -10 \text{ dB}, \quad \omega C_s Z_0 [2 - \omega^2 C_g L + C_g/C_s + R_i/Z_0 (1 + C_g/C_s)] \ll 1$$

Equations (2)–(3) are matching, and insertion loss at ON-state and Equation (5) is isolation in OFF-state. Deviation between simulated and insertion loss is mostly due to contact contamination during testing in non-hermetic environment.

5. RELIABILITY MEASUREMENTS OF SWITCHES: PHASE IV

Complete reliability test setup is shown in Figure 7(a). Amplified RF signals of different power level (0.1–1 W) at 2.4 GHz is applied to the device under test (DUT). A power meter is connected with a 20 dB directional coupler to monitor the power level of incoming RF signal. Switches and phase shifters are controlled using a bias waveform shown in Figure 7(b). Waveform is formed with 60 μ sec period and follows a ramp with 15 μ sec rise time and 10 μ sec fall time. The amplitude of the dc waveform is set to +100 V, and 25 μ sec time span is maintained during the contacting period. To monitor the contact resistance (R_c) changes over lifetime, a four-point resistance measurement setup is connected with bias tee. The output RF signal is captured through a directional coupler to the RF detector. A temperature controller is connected with probe station to observe the device performances at different operating temperatures from 25°C to even up to 85°C, as shown by Block 2 in Figure 7(a). In the first case, variation of single switch R_c is measured, and it is found from 1.9 to 1.81 Ω with 89–100 V bias at 0.1 W RF power, as shown in Figure 8. The experiment is verified by fitting the measured 2-port S -parameter data in a switch equivalent circuit model, presented in Figure 3(b). Switch actuation area is increased at higher bias voltage, and contact resistance (R_c) decreases. It has been observed and

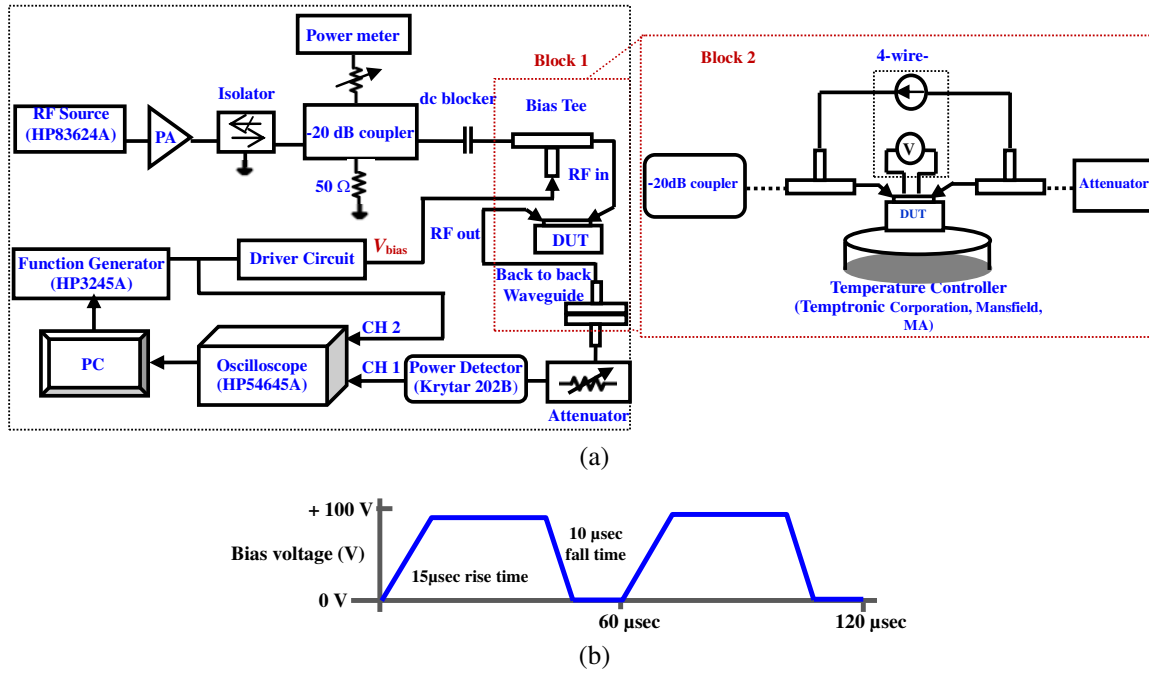


Figure 7. (a) Test set up and (b) bias waveform for reliability characterization.

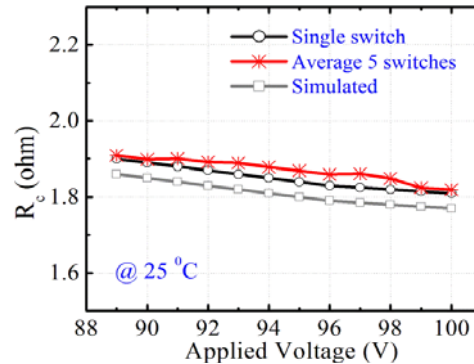


Figure 8. Measured contact resistance versus applied voltage for single lateral MEMS switch.

ensured from the measurement that switch takes ~ 137 V to reach the critical or pull-in limit. Hence, 100 V is a safe limit and is used in all fabricated switches.

Initially single lateral switch is measured, and it shows excellent performances even up to 1 billion (B) cycles. R_c of the switches are measured utilizing the setup depicted in Figure 7(a) at 25°C with 0.5 W, 0.8 W and 1 W of incident RF power level, as shown in Figure 9. R_c variation from 1.89–3.5 Ω, 2.14–3.98 Ω, 2.49–4.97 Ω, and 2.84–6 Ω are obtained up to 1 B cycle from SPST, SPDT, SP3T, and SP6T switches, respectively, with 0.5–1 W of RF power, as shown in Figures 9(a)–9(d). The variation of R_c is mostly due to contact contaminants with excessive temperature rise on contact at higher power in the non-hermetic conditions. Note that test is stopped after 1 B cycle. The insertion loss variation in last cycle with 1 W of RF power is shown in Figure 10. Result shows SPST switch loss of 0.49 dB (3.78 dB), SPDT switch loss of 0.7 dB (4.1 dB), SP3T switch loss of 0.83 dB (4.67 dB), and SP6T switch loss of 1.6 (5.8 dB) at 3.5 GHz (28 GHz) with 1 W of RF power. The test is performed up to 1 B cycles to check whether the device is operational or not in terms of self actuation or contact point degradation. The change in loss is mostly due to ohmic loss from contact heating. A comparison of the proposed switches with other reported switches is presented in Table 1 for completeness.

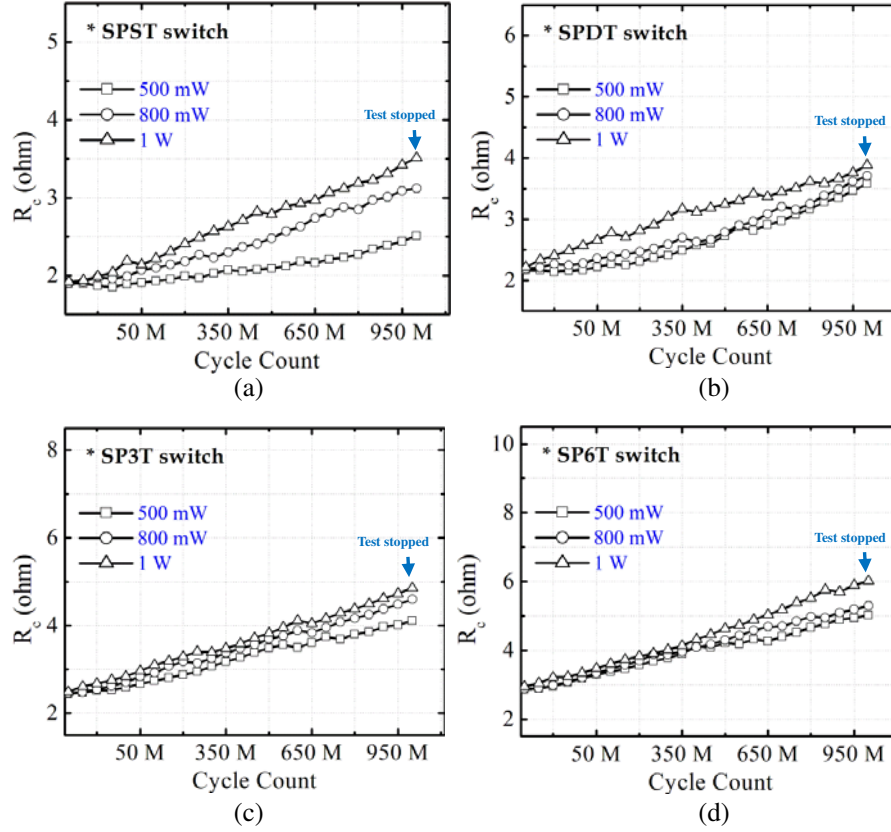


Figure 9. Variation of R_C as a function of cycle count with three different incident power levels at 25°C for (a) SPST, (b) SPDT, (c) SP3T and (d) SP6T switching networks.

Table 1. Performance comparisons of MEMS based SP_nT switching networks (SPDT, SP3T and SP6T).

SP n T switches (SPDT, SP3T, SP6T)	Loss (dB)	Isolation (dB)	Area (mm ²)	Reliability cycles
SPDT [2], at 20 GHz	2.05	36	NA*	NA*
SPDT [1], at 5 GHz	0.08	32	1.8	NA*
SPDT [4], at 20 GHz	1.67	42	1.72	200 k
This work at 3.5 GHz	0.42	42	0.25	>1B at 1W
This work at 28 GHz	3.3	28.7	0.25	>1B at 1W
SP3T [1], at 15 GHz	0.7	20	2.45	NA*
SP3T [4], at 12 GHz	0.35	20	0.43	1B at 1W
This work at 3.5 GHz	0.37	33	0.36	>1B at 1W
This work at 28 GHz	3.89	22	0.36	>1B at 1W
SP6T [5], at 6 GHz	0.7	39	1	NA*
SP6T [4], at 12 GHz	0.7	18	0.58	1B at 1W
This work at 3.5 GHz	1.1	31	0.7	>1B at 1W
This work at 28 GHz	5	17.7	0.7	>1B at 1W

*NA: Not Available

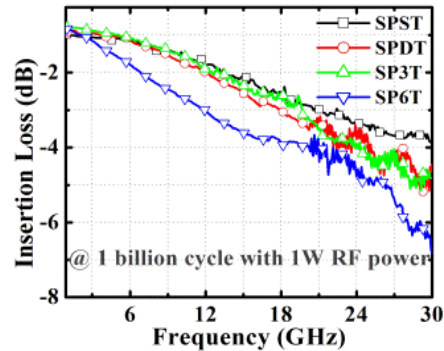


Figure 10. Measured reliability performances in terms of loss from all switches at 1B cycles from 1 to 30 GHz at 25°C with 100 V bias voltage.

6. CONCLUSION

We have proposed and implemented high reliable (>1B cycles), moderate power (1W) and compact (maximum area is 0.7 mm²) MEMS based switching networks up to SP6T utilizing electrostatically driven lateral MEMS switches. All switches are operated well till up to 30 GHz, and performances are optimized and demonstrated at 3.5 GHz and 28 GHz for 5G applications. The variation of switch contact resistance with cycle count is presented and discussed in details. Authors believe that device performances could be improved further with well suited contact material like rhodium or gold-palladium alloys. Note that actuation voltage of the proposed switch is in higher sides. It can be decreased using thin metal layer, but it may affect the reliability. Another option is to adopt the silicon-on-insulator process where a thin layer of the switch can be made with CPW (Si-core CPW) [1]. Otherwise, a charge pump circuit must be used with the proposed switch for practical applications. Switching network performances at higher temperature will be studied in future.

ACKNOWLEDGMENT

The first two authors would like to express their profound gratitude to the Synergy Microwave Corp, NJ, USA and Science and Engineering Research Board (SERB), Govt of India under project no: ECR/2018/002258.

REFERENCES

1. Liu, A. Q., *RF MEMS Switches and Integrated Switching Circuits*, Springer, New York, Mar. 2010.
2. Yamane, D., W. Sun, H. Seita, S. Kawasaki, H. Fujita, and H. Toshiyoshi, "A Ku-band dual-SPDT RF-MEMS switch by double-side SOI bulk micromachining," *Journal of Microelectromechanical System*, Vol. 20, No. 5, 1211–1221, 2011.
3. Dey, S. and S. K. Koul, "Systematic measurement of high isolation DC-20 GHz miniature MEMS SPDT switch," *Microw. and Opti. Techno Lett.*, Vol. 58, No. 5, 1154–1159, 2016.
4. Dey, S., S. K. Koul, A. K. Poddar, and U. L. Rohde, "Extensive performance evaluations of RF MEMS single-pole-multi-throw (SP3T to SP14T) switches up to X-band frequency," *J. Micromech. Microeng.*, Vol. 27, No. 1, 1–9, 2016.
5. Lee, J., C. H. Je, S. Kang, and C. A. Choi, "A low-loss single-pole six-throw switch based on compact RF MEMS switches," *IEEE Trans. Microw. Theory Techn.*, Vol. 53, No. 11, 3335–3344, 2005.
6. Koul, S. K., S. Dey, A. K. Poddar, and U. L. Rohde, "Reliable and compact 3-bit and 4-bit phase shifters using MEMS SP4T and SP8T switches," *IEEE J. Microelectromech. Syst.*, Vol. 27, No. 1, 113–124, 2018.